Automatic Segmentation of Micro CT Images

ME EN 6035 Final Project

Nik Benko and Peter Creveling

April 29, 2018

Abstract

In this study, the accuracy of automatic segmentation methods were statistically compared to a manual segmentation method. Segmentation was performed on μCT images of fiber-reinforced ceramic matrix composites in order to extract porosity from the surrounding microsctucture. Four different automatic segmentation methods were investigated. Statistical analysis was performed to determine how the methods compared. It was found that using a combination of pre-segmentation filtering, 3D machine learning segmentation, and post-process edge erosion had the best agreement with manual segmentation.

1 Introduction and Background

Fiber-reinforced ceramic matrix composites (CMCs) are widely used in the aerospace industry due to their high specific strength, high stiffness, and their ability to withstand prolonged exposure to extreme high-temperature and oxidative environments. Despite their increased use, the physics governing their manufacturing, stochastic microstructure, and long-term structural performance remains an active area of research. Understanding the complete life-cycle of CMCs is critical towards improving existing and future applications of CMCs. In recent years, the emerging practice of in situ X-ray micro-computed tomography (X-ray μCT) experiments has proven useful for providing a holistic understanding of the behavior of CMCs on multiple length scales [1–6].

Unique to X-ray μCT is the ability to take through-thickness images of specimens in 3-D. This provides much more information compared to other 2-D surface based techniques. However, processing these images to extract information comes at high computational costs. One of the most common imaging processing operations is segmentation, in which pixels are categorized into two more groups that correspond to some characteristic of the material being imaged. For example, CMC images are often segmented to distinguish between fibers and the surrounding matrix. There exist active areas of research in improving best practices for the segmentation

of X-ray μCT reconstructions. Segmentation techniques vary widely depending on image properties such as noise characteristics, contrast between segments, and edge sharpness. X-ray μCT of large specimens on the order of tens of millimeters results in an image with a significant signal to noise ratio, making automatic segmentation challenging. Researchers have largely relied on manual segmentation, in which a user classifies each pixel by hand. While accurate, this method is very time consuming and impractical for processing of large data sets as well as being difficult to reproduce. For this reason the development of an automated method of segmentation is desired.

In this study, several automatic segmentation strategies were constructed and tested against a manually segmented data set to determine accuracy. Slices of a 3-D X-ray μCT image data set were segmented to calculate the porosity of each slice. Porosity was defined as the number of pixels representing materials other than carbon fibers or the surrounding matrix, divided by the total number of pixels in the image. A statistical validation was performed to compare the differences in segmentation ability between the automatic methods and the manual segmentation method.

2 Materials and Methods

2.1 Composite CMC and X-ray μCT

This study is an extension of current research being performed in the Utah Composites lab where X-ray μCT is being utilized to image the entire multi-step manufacturing process of CMCs combined with *in situ* testing during extreme environments. The end goal is to fully quantify the changes of the CMC microstructure throughout their entire life-cycle via methods of segmentation. The composite system used consisted of a 8HS satin weave CG Nicalon-fiber fabric infiltrated with SMP-10 matrix. Imaging was performed using a Zeiss Versa-520 X-ray CT 3D microscope at the Air Force Research Laboratory (Dayton, OH). In this study, images were analyzed from the pyrolysis step of the manufacturing process after which the resin was cured at 1000°C.

2.2 Data

Images were collected with a scan time of 37.3 hours about a selected region of interest (ROI) from the center of the entire CMC specimen with dimensions of 60×30×1.5 mm. There were 1980 8-bit images collected with a spatial resolution of 1.21 μm/voxel. In total, the entire image stack consisted of 22.1GB of information. For this study, a small sub-volume of 500×500×500 pixels was analyzed. Within this sub-volume, both manual and automatic segmentation were performed in order to extract porosity (e.g. cracks or voids) from the surrounding microstructure. It was assumed that the manual segmentation based method of porosity is the "ground truth" to compare the accuracy of the automatic segmentation.

2.3 Automatic Segmentation Methods

The automatic segmentation methods consisted of a pre-processing step using a non-local-means filter. This was performed to remove an optimal amount of noise induced by the X-rays due to the large specimen geometry while maintaining image fidelity of the material microstructure. Next, a machine learning algorithm known as WEKA segmentation was implemented to segment out individual pixels corresponding to porosity. This algorithm utilizes a combination of data mining, clustering, classification, regression, visualization, and feature selection to perform the desired segmentation [7–10]. WEKA can be utilized on both 2-D discrete images as well as 3-D image stacks. Both 2-D and 3-D techniques were executed on the filtered data. From preliminary results as described later in section 3, a method known as Edge Erosion was implemented to attempt convergence between automatic segmentation results and manual segmentation due to the over-prediction of porosity edges. In total, there were four automatic segmentation methods executed, 2-D and 3-D WEKA segmentation of the filtered image stacks as well as 2-D and 3-D WEKA segmentation plus Edge Erosion of the filtered image stacks.

2.4 Statistical Analysis

Several different statistical techniques were used to evaluate segmentation algorithms. First a one-way ANOVA was conducted on the porosity measurements for each technique to determine whether or not automatic calculations of porosity were significantly different from manual calculations. Here the null hypothesis is that all methods result in the same mean porosity measurement for the image set. They alternative hypothesis is that some means are not equal. A multiple comparisons analysis (Tukey's HSD) was then conducted to test multiple alternative hypothesis and determine which methods, if any, were statistically different.

An additional data set was constructed by calculating the percent error between each of the automatically segmented results and the manually segmented results. This data was no longer dependent on the underlying image and could be treated as a random variable. Normality of data was checked by plotting the histograms for each automatic method. Finally, the four automatic methods segmentations were broken into two categories based on algorithm features with "high" and "low" treatments for each category. A 2 by 2 factorial and 2-way ANOVA were performed to determine which algorithm features, Analysis Dimensions and Edge Erosion, most effected the results.

3 Results and Discussion

Histograms of the porosity calculations are shown in Figure 1. The histograms reveal that most data sets do not meet the condition of normality and contain a heavy left skew. This is in fact not surprising as the porosity measurement is based on image content, which is not a

random variable. Mean porosity and standard deviation (STD) are listed in Table 1. Results from the one-way ANOVA 2 and multiple comparisons **??** test show that there are significant differences in the means of all of the methods except between the manual segmentation and 3-D algorithm with Edge Erosion correction.

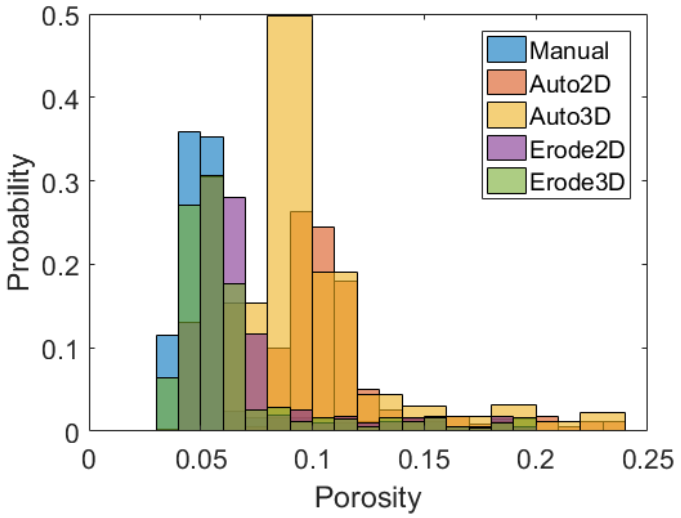

Figure 1: Histogram of porosity distribution for each segmentation method

Table 1: Porosity Calculations

Method	Manual	2D	3D	2D EE	3D EE
Mean	0.0599	0.1143	0.1035	0.0715	0.0651
STD	0.0316	0.0322	0.0341	0.0311	0.0334

Table 2: One Way ANOVA Results

Source	SS	DF	MS	F	P
Group	1.8878	4	0.29719	281.14	0
Error	2.63218	2490	0.00106		
Total	3.82096	2494			

Histograms of percent error calculations in Figure 2 show that these data are normally distributed. This difference, with respect to the distribution of raw porosity data, can be understood by considering that the percent difference is no longer highly dependent on the image content, but rather on the segmentation method. This allows the percent error to be considered a random variable for further analysis. Mean error and standard deviation are listed in Table 3. As expected from the prior analysis, the 3-D with edge erosion algorithm displayed the lowest error and standard deviation, indicating that it is the desired method of analysis.

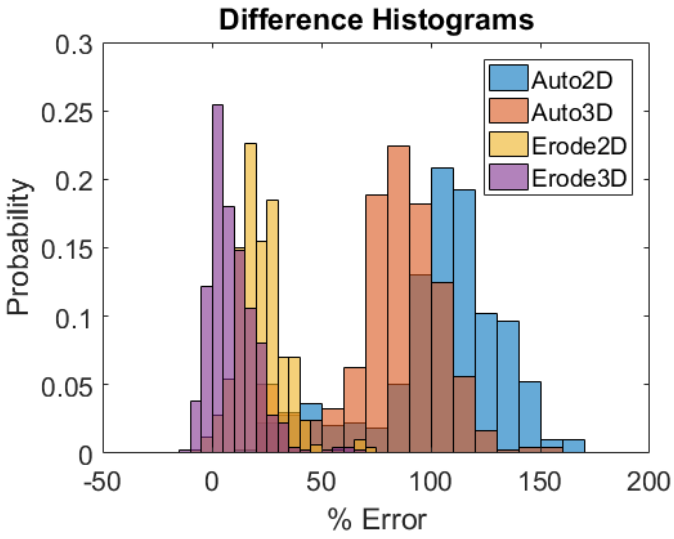

Figure 2: Histogram of percent error for each of the automatic segmentation methods

Table 3: Percent Error Calculations

Meathod	2D	3D	2D EE	3D EE
Mean	104.21	82.56	22.33	9.22
STD	29.05	23.18	11.21	11.00

Finally, the factorial analysis resulted in the following

linear regression equation:

$$PercentError = 54.5790 - 8.6906X_A - 38.8059X_B + 2.1367X_AX_B \quad (1)$$

Where X_A and X_B represent the coded variables for analysis dimension and edge erosion respectively. A response surface is plotted in Figure 3. This analysis shows that the pixel erosion contributes more to segmentation accuracy than the dimensionality of the Weka segmentation algorithm. This result could be useful for applying these techniques to larger data sets where computer memory becomes a limiting factor for 3-D methods. The results of the two-way ANOVA in Table 4 show that all effects measured in the factorial analysis were statistically significant.

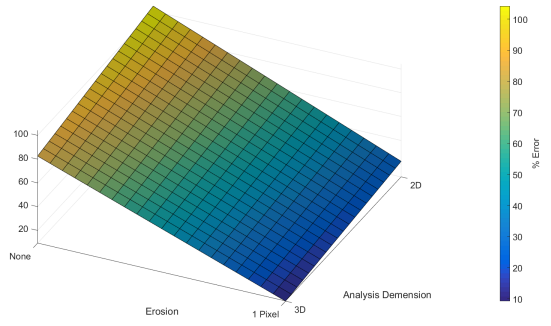

Figure 3: Response surface model for two different algorithm features

Table 4: Two Way ANOVA for factorial analysis

Factor	SS	DF	MS	F	P
Dimensionality	15.08	1	15.08	370.4	0
Edge Erosion	300.58	1	300.58	7386.0	0
Interaction	0.911	1	0.911	22.39	0
Error	81.07	1992	0.041		
Total	397.63	1995			

3.1 Error and Uncertainties

Image analysis and segmentation are inherently prone to error. Digital imaging captures light reflected by, or transmitted through a continuous media and records discretized values of light intensity. If image discretization does not exactly match boundaries within the image subject, distortion and blurring of edges will occur. Image noise further confounds the distinction of image contents. The human visual system is effective at interpreting image contents, but interpretation can vary widely from person to person.

The analysis here used manually segmented images as a "ground truth" for comparison between methods, but the chosen segmentation could have easily contained slight variations if another person had conducted the segmentation. The attractiveness of automatic segmentation lies in both its speed *and* repeatability. Until imaging tools are capable of producing sharp enough images that there are no questionable "edge cases" for segmentation, there will always remain some small unquantifiable uncertainty in segmentation methods. However, by using the same algorithm across data sets for the purpose of comparison, this uncertainty can be ignored because it is present in all data sets.

4 Conclusion and Future Directions

In summary, this work demonstrates the ability of an automatic segmentation algorithm to produce results with no statistically significant differences from a manually segmented μCT image data set. Average error of less than 10% was achieved. It is possible that this value can be further reduced by additional training to the underlying machine learning architecture. Pixel erosion was shown to be an effective method to compensate for the architecture's tendency to over-predict image porosity. Future work will include additional testing of the algorithms presented here on full-volume data sets.

References

[1] N. Larson and F. Zok, "In-situ 3d visualization of composite microstructure during polymer-to-ceramic conversion," *Acta Materialia*, vol. 144, pp. 579–589, 2018.

[2] H. Bale, A. Haboub, and et al., "Real-time quantitative imaging of failure events in ultrahigh-temperature materials under load at temperatures above 1600c," *Nature Materials*, vol. 12(1), pp. 40–46, 2013.

[3] H. Bale, M. Blacklock, and et al., "Characterizing three-dimensional textile ceramic composites using synchrotron x-ray computed micro-tomography," *Journal of the American Ceramic Society*, vol. 95, pp. 392–402, 2012.

[4] B. Cox, H. Bale, and et al., "Stochastic virtual tests for high-temperature ceramic matrix composites," *Annual Review of Materials Research*, vol. 44, pp. 479–529, 2018.

[5] A. Haboub, H. Bale, and et al., "Tensile testing of materials at high temperatures above 1700 c with in situ synchrotron xray micro-tomography," *Review of Scientific Instruments*, vol. 85.8, p. p.083702, 2014.

[6] D. Marshall and B. Cox, "Integral textile ceramic structures," *Annual Review of Materials Research*, vol. 38, pp. 435–443, 2008.

[7] S. Cunningham and P. Denize, "A tool for model generation and knowledge acquisition," in *Proc International Workshop on Artificial Intelligence and Statistics*, (Fort Lauderdale, Florida, USA), pp. 213–222, 1993.

[8] G. Holmes and S. Cunningham, "Using data mining to support the construction and maintenance of expert systems," in *Proc Artificial Neural Networks and Expert Systems*, (Dunedin, New Zealand), pp. 156–159, 1993.

[9] G. Holmes and S. Cunningham, "Expert systems development using data mining," in *Proc Expert Systems '93*, (Cambridge, England), pp. 213–222, 1993.

[10] I. Witten, S. Cunningham, G. Holmes, R. McQueen, and L. Smith, "Practical machine learning and its

potential application to problems in agriculture,"
in *Proc New Zealand Computer Conference*, vol. 1,
(Auckland, New Zealand), pp. 308–325, 1993.